Dynamic stability of natural circulation loops for single phase fluids with internal heat generation

D. E. Ruiz [a], A. Cammi [b], L. Luzzi [b,*]

[a] Princeton University, Department of Astrophysical Sciences, Princeton, NJ 08544, USA
[b] Politecnico di Milano, Department of Energy, CeSNEF (Enrico Fermi Center for Nuclear Studies), via La Masa 34, 20156 Milano, Italy

Received 4 August 2014
Received in revised form
2 December 2014
Accepted 17 December 2014
Available online 1 January 2015

1. Introduction

In a natural circulation loop, the circulating fluid removes heat from a source and transports it to a heat sink. The driving force is the fluid buoyancy force. In a closed loop, steady state natural circulation is achieved when the driving buoyancy forces are in balance with the frictional forces. However, under certain circumstances, the achieved steady state can be dynamically unstable. The possible instabilities can lead to large oscillations in the fluid flow and on the temperature field and cause an inconvenient operation of the closed loop system. Since natural circulation has gained importance in many engineering applications, such as in the chemical and nuclear engineering communities, it is important to determine the dependence of the stability maps on the external parameters (IAEA, 2005).

Natural circulation loop instabilities have been studied both theoretically and experimentally. The first theoretical studies on the subject were presented by Keller (1966) and Welander (1967). Further theoretical studies have focused on the stability analysis for different loop geometries (Chen, 1985; Swapnalee and Vijayan, 2011; Vijayan et al., 2007, 2008). Using another approach, stability analysis of thermosyphon loops was studied via finite difference methods (Ambrosini and Ferreri, 1998, 2000; Misale et al., 2000). On the other hand, the first experimental studies on the subject were done by Creveling et al. (1975) and Gorman et al. (1986). Subsequent experimental studies have been performed by Vijayan et al. (2007), Swapnalee and Vijayan (2011), and others. These works have studied in detail natural circulation in a variety of closed loop configurations in which there is an external heat source and an external heat sink. However, no attention has been given to single-phase natural circulating flows with internally heated fluids (Pini et al., 2014).

This work studies oscillating instabilities in closed single-phase thermosyphon loops when internal heat generation is present. Until now, it is unknown how the stability of closed natural circulation loops is affected when internal heat generation effects are considered. A fluid with internal heat generation might be, for

* Corresponding author. Tel.: +39 02 2399 6326.
E-mail address: lelio.luzzi@polimi.it (L. Luzzi).

example, a fluid with internal exothermic chemical reactions or a molten salt fuel in a nuclear Molten Salt Reactor (MSR) (GIF, 2013; Serp et al., 2014). In MSRs, fission products decay inside the molten salt and release energy (Di Marcello et al., 2010; Fiorina et al., 2014; Luzzi et al., 2012, 2010). Other examples of fluids with internal heat generation might include fluids heated via electrical currents (ohmic heating). It is believed that the study of natural circulation of internally heated fluids may concern a number of engineering domains.

In the present paper, two methods were used in order to calculate the stability maps of the investigated natural circulation loops: a semianalytical linear method and a numerical nonlinear method. These methods were applied to investigate the stability of two closed loop configurations: the Vertical Heater - Horizontal Cooler (VHHC) and the Vertical Heater - Vertical Cooler (VHVC) configurations. In these circuits, the heat sink position and orientation are varied.

The present work is organized as follows. Section 2 presents the general procedures and mathematical tools used for the stability analysis. In Section 3, the obtained stability analysis methods are applied to study the dynamical stability of the VHHC and VHVC circuit loops. In Section 4, the main results are presented and discussed. Concluding remarks are given in Section 5.

2. General stability analysis methods

In the present section, the methods for performing the stability analysis are presented. The developed model allows for both external heating and internal heat generation. The section is organized as follows: first, a general description of the system with the governing equations is presented. Then, the procedure for determining the steady state is given. Finally, the linear stability analysis and the numerical nonlinear stability analysis methods are presented.

2.1. System description and governing equations

In this work, the closed loop configurations studied are composed of a single "heater" and a single "cooler" in a closed rectangular loop with a circular tube cross-section of constant diameter (see Fig. 1). In this configuration, the cooler length is denoted as L_c. The tube section connecting the "cooler" with the "heater" is called the "cold leg" of length L_{cl}. The length of the "heater" is denoted L_h. Finally, the tube section transporting the hot fluid from the "heater" to the "cooler" is called the "hot leg" of length L_{hl}. The total length of the circuit is $L_t \doteq L_c + L_{cl} + L_h + L_{hl}$.[1] This general notation to designate the sections of the closed-loop circuit will be used throughout the work.

The system governing equations refer to an incompressible fluid, with the following additional assumptions:

- The fluid flow is considered one-dimensional. The curvilinear coordinate "s" denotes the position inside the closed loop, and it follows the direction of the fluid flow. The origin is taken at the entrance of the system heat sink or "cooler".
- The Boussinesq approximation is considered. A linear variation of the fluid density due to temperature change is considered in the gravitational term of the conservation of momentum equation.
- Two heat sources are included. The first heat source is that of the system external heater (this could be an electrical heater in a test-loop facility or a nuclear reactor). The second heat source is the fluid internal heat generation, which is considered uniform inside the circuit.[2]
- The system heat sink is modeled as a constant wall temperature cooler.
- Dissipative terms of the energy conservation equation are neglected.
- Heat conduction inside the fluid is neglected.
- It is supposed that the circuit has constant diameter D.
- Regarding the pressure losses due to friction inside the circuit, it is supposed that the same flow regime (laminar or turbulent) exists for the whole circuit. Also, the fluid dynamic viscosity, μ, is supposed to be constant along the circuit. The previous two assumptions were relaxed in the work of Vijayan et al. (2008).

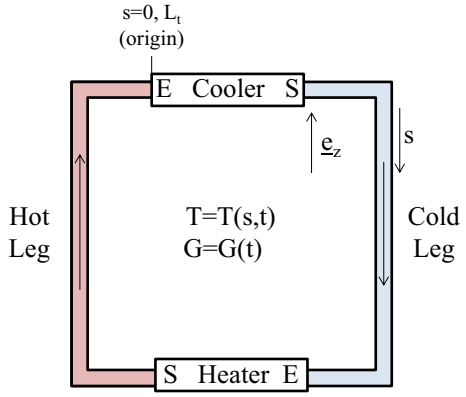

Fig. 1. General schema of a natural circulation closed loop. The symbols "E" and "S" denote the entrance and exit cross-sections, respectively.

Throughout the present work, the velocity of the fluid is defined as $\underline{v} \doteq v\underline{e}_s(s)$, where $\underline{e}_s(s)$ is the unit vector of the flow and $v \geq 0$. The governing equations with the above assumptions are

$$\frac{\partial G}{\partial s} = 0, \tag{1}$$

$$\frac{\partial G}{\partial t} + \frac{\partial}{\partial s}\left(\frac{G^2}{\rho^*}\right) = -\frac{\partial p}{\partial s} - \rho g \underline{e}_z \cdot \underline{e}_s - \frac{1}{2} f \frac{G^2}{\rho^*}\frac{1}{D}, \tag{2}$$

$$\rho^* c_p \frac{\partial T}{\partial t} + G c_p \frac{\partial T}{\partial s} = \begin{cases} -\overline{h}(T - T_w)\dfrac{P}{A} + q''' & \text{cooler} \\ q''\dfrac{P}{A} + q''' & \text{heater} \\ q''' & \text{otherwise} \end{cases}, \tag{3}$$

$$\rho(T) = \rho^*\left[1 - \beta(T - T^*)\right], \tag{4}$$

where $\rho^* \doteq \rho_0(s=0)$ is the reference density (taken at the cooler entrance) at steady state, $G(t) \doteq \rho^* v$ is the mass flux, $T(s,t)$ is the fluid temperature field, β is the thermal expansion coefficient, $f \doteq a/Re^b$ is the Darcy friction factor, T_w is the cooler wall temperature, c_p is the fluid specific heat, D is the diameter of the circuit, P is the perimeter of the tube, A is the area of the tube cross-section, and $\overline{h}$ is the heat transfer coefficient.

It is important to notice that in Eq. (3) there are two heat source terms. The first source term denoted by q'' represents the

[1] Throughout this paper, we denote $a \doteq b$ meaning that "a" is defined as "b".

[2] For nuclear applications with circulating-fuel MSRs, it is well known that for nominal operating conditions the decay heat varies by a small percentage inside the circuit. The strongest decay heat release takes place inside or immediately outside the core and is caused by the fastest decaying fission products. During emergency or accidental conditions, in which the nuclear core is shut down, the decay heat may be considered uniform.

constant heat flux injected into the system by the heater. The second source term, q''', represents the fluid internal heat generation (considered uniform inside the loop). The scope of this work is to investigate how this last term affects the stability of natural circulating flows.

2.1.1. Friction factor

Natural circulation flow covers from laminar to turbulent flow conditions. At low thermal powers, the fluid flow would tend to be small and could be laminar. In this case, the Darcy friction factor is $f_{laminar} = 64/Re$. For high Reynolds numbers, the fluid flow is turbulent, and the friction factor can be evaluated as follows: $f_{turbulent} = 0.316/Re^{0.25}$ (De Nevers, 1970).

The region covering the transition between laminar and turbu-lent is not very well known. For a straight-infinite tube flow, the transition zone is considered to be at $Re \sim 2000$. For closed loop natural circulation flows, the transition has been reported to be as low as $Re \sim 340$ (Hallinan and Viskanta, 1986; Swapnalee and Vijayan, 2011). In order to model the transition from laminar to turbulent regimes, some authors have defined a transition Reynolds number (e.g., as the Re value in which the laminar and turbulent correlations intersect Vijayan et al., 1995). A more detailed description of the modeling of the friction factor in Swapnalee and Vijayan (2011).

Although many models use piecewise-defined functions for the friction factor that are continuous, their derivatives at the transition points are not continuous. This inconvenience brings discontinuities in the stability maps, which will be explained later in Section 4. In order to solve this problem, this work uses a continuous and derivative continuous friction factor that covers from laminar to turbulent flow conditions. The friction factor was built by fitting experimental steady-state data on fluid flow inside a straight infinite tube (Perry and Green, 2008). The developed correlation is

$$f \doteq \frac{a}{Re^b}, \tag{5}$$

where

$$a \doteq 64^{\gamma} 0.316^{1-\gamma}, \tag{6}$$

$$b \doteq \gamma + (1-\gamma)0.25, \tag{7}$$

$$\gamma(Re) \doteq \frac{1}{1+\exp\{(Re-2530)/120\}}. \tag{8}$$

The correlation uses a "Fermi–Dirac distribution" factor, γ, to model the transition between laminar and turbulent flows. By taking the asymptotic limits of γ in Eqs. (5)–(8), the proposed correlation converges towards the laminar and turbulent friction factors:

$$f_{laminar} = \lim_{Re \to 0} f \simeq 64/Re,$$
$$f_{turbulent} = \lim_{Re \to +\infty} f = 0.316/Re^{0.25}.$$

Fig. 2 compares the proposed correlation (5) with the Churchill experimental data points for the friction factor. As it can be seen, the proposed correlation closely fits the transition zone while also having a continuous derivative. This friction correlation will be used throughout the present work.

2.2. Stationary state

For closed loops composed of only one heater and one cooler, the stationary temperature distribution can be written in a general form. By using Eqs. (1)–(3), the stationary temperature distribution is

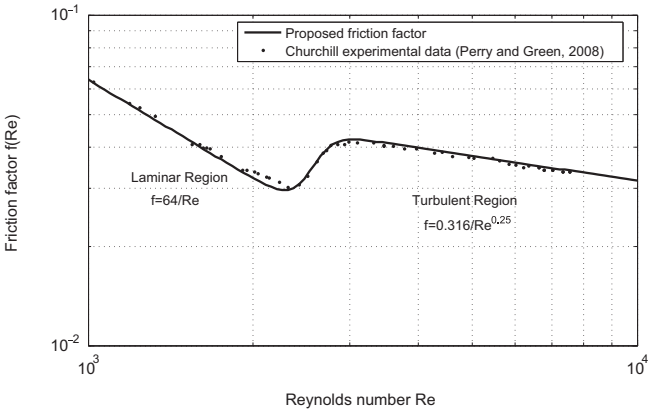

Fig. 2. Friction factor correlation.

given by

$$T_0(s) = \begin{cases} T_0(s=0) + \left[T_w + q''' \dfrac{A}{\overline{h}P} - T_0(s=0)\right] & \\ \quad \times \left[1 - \exp\left(-\dfrac{\overline{h}P}{G_0 c_p A} s\right)\right] & \text{cooler} \\ T_0(L_c) + \dfrac{q'''}{G_0 c_p}(s - L_c) & \text{cold leg} \\ T_0(L_c) + \dfrac{q'''}{G_0 c_p}(s - L_c) & \\ \quad + \dfrac{q''}{G_0 c_p}\dfrac{P}{A}(s - L_c - L_{cl}) & \text{heater} \\ T_0(L_c) + \dfrac{q'''}{G_0 c_p}(s - L_c) + \dfrac{q''}{G_0 c_p}\dfrac{P}{A} L_h & \text{hot leg} \end{cases}, \tag{9}$$

where $T_0(s=0)$ is the stationary temperature at the cooler entrance, G_0 is the stationary mass flux, and $T_0(L_c)$ is the temperature of the fluid at the cooler exit. As shown, the calculated temperature distribution respects continuity between the various sections of the loop. As boundary condition for the temperature field, T_0 must be continuous at $s=0$ and $s = L_t$:

$$T_0(s=0) = T_0(s=L_t) \tag{10}$$

$$\Longrightarrow T_0(s=0) = T_w + q''' \frac{A}{\overline{h}P} + \frac{\Delta T_{heater} + \Delta T_{int}}{1 - \exp(-\varphi L_c)},$$

with

$$\varphi \doteq \frac{\overline{h}P}{G_0 c_p A} = \frac{4Nu}{RePr}\frac{1}{D} = 4\, St \frac{L_t}{D}\frac{1}{L_t} = St_m \frac{1}{L_t},$$

$$\Delta T_{heater} \doteq \frac{q''}{G_0 c_p}\frac{P}{A} L_h,$$

$$\Delta T_{int} \doteq \frac{q'''}{G_0 c_p}(L_t - L_c), \tag{11}$$

where φ is the Stanton number St_m divided by the total length of the circuit, ΔT_{heater} is the temperature variation of the fluid caused by the surface heat flux inside the heater, and ΔT_{int} is the temperature variation caused by the internal heat generation term outside the heat sink. In other words, ΔT_{int} is the temperature difference between the cooler entrance and exit when only internal heat generation is present. From these calculations, a typical steady-state temperature distribu-tion from Eq. (9) is shown in Fig. 3 as an example.

In Eq. (9), the temperature field is obtained in terms of the steady-state flux G_0. The flux G_0 can be determined using the conservation equation of momentum. Eq. (2) is integrated over the

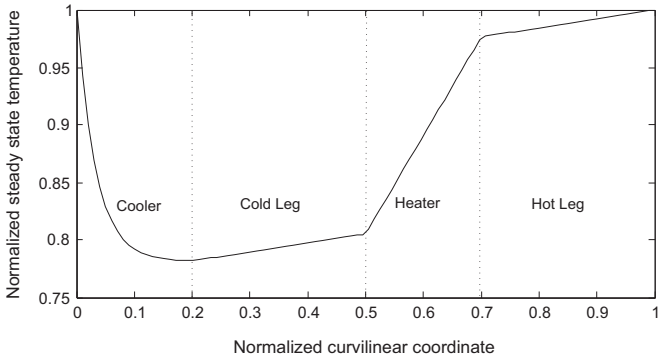

Fig. 3. Example illustrating a steady-state temperature field.

entire loop in order to eliminate the pressure variable:

$$\frac{1}{2}f_0\frac{G_0^2}{\rho^*}\left[\frac{L_t}{D}+\sum_{j=1}K_j\right]=\rho^* g\beta\oint T_0(s)\underline{e}_z\cdot\underline{e}_s(s)\,\mathrm{d}s, \tag{12}$$

where K_j is a factor allowing for the local pressure losses inside the circuit. The line integral of the temperature distribution depends on the loop geometry. Since the total temperature variation outside the cooler is due to the heat introduced by the external heater and the internal heat generation, the line integral of the steady state temperature field is written as

$$\Delta T_{heater}\mathcal{L}_{heater}+\Delta T_{int}\mathcal{L}_{int}\doteq\oint T_0(s)\underline{e}_z\cdot\underline{e}_s(s)\,\mathrm{d}s, \tag{13}$$

where the $\mathcal{L}_{heater}$ and $\mathcal{L}_{int}$ factors depend only on the loop geometry and the direction of the flow (clockwise or counterclockwise). We now introduce the following variables:

$$\Delta T_0\doteq\Delta T_{heater}+\Delta T_{int},\quad \alpha\doteq\Delta T_{heater}/\Delta T_0, \tag{14}$$

where ΔT_0 is the total change of the fluid temperature at steady-state, and $\alpha\in[0,1]$ is related to the ratio of the heating power inside the heater to the total heating power. Hence, it is possible to write Eq. (12) as

$$\frac{1}{2}f_0\frac{G_0^2}{\rho^*}\left[\frac{L_t}{D}+\sum_{j=1}K_j\right]=\rho^*\beta g\Delta T_0[\alpha\mathcal{L}_{heater}+(1-\alpha)\mathcal{L}_{int}]. \tag{15}$$

The variable α will be particularly important for the remainder of this work. Modifying α changes the relative ratio between the heat inserted by the external heater and the heat coming from the internal heat generation. To further illustrate this, $\alpha=1$ represents a situation in which no internal heat generation is considered ($q'''=0$). The convection movement is driven by the thermal energy introduced by the heater. When $\alpha=0$, the heat is only supplied internally by the fluid. It is later shown in Section 4 that the circuit stability maps depend strongly on the parameter α.

In the literature, a convenient dimensionless group used to express Eq. (15) is using the modified Grashof number and the Reynolds number (Vijayan, 2002; Vijayan et al., 2007). Eq. (15) can be hence written as

$$\frac{a}{2}Re_0^{3-b}\left[\frac{L_t}{D}+\sum_{j=1}K_j\right]=Gr_m, \tag{16}$$

where Gr_m is the modified Grashof number which is defined as

$$Gr_m\doteq\frac{\rho^{*2}gD^3}{\mu^2}\beta\Delta T_m. \tag{17}$$

The modified total temperature variation ΔT_m is defined as

$$\Delta T_m\doteq\frac{G_0}{\mu}[\Delta T_{heater}\mathcal{L}_{heater}+\Delta T_{int}\mathcal{L}_{int}]. \tag{18}$$

It is important to state that besides the approximations used when writing Eqs. (1)–(3), the solutions obtained in Eqs. (15) and (16) do not have other approximations. The only terms left to be calculated are $\mathcal{L}_{heater}$ and $\mathcal{L}_{int}$, which are obtained when specifying the loop geometry and the flow direction.

The field variables G and T are perturbed around the stationary solution:

$$\begin{aligned}&G(t)=G_0+G_1(t),\quad G_1(t)\ll G_0\\&T(s,t)=T_0(s)+T_1(s,t),\quad T_1(s,t)\ll T_0(s).\end{aligned} \tag{19}$$

The perturbed variables G and T are inserted inside Eqs. (2)–(4). When neglecting second-order terms, the following linear time-dependent equations are obtained[3]:

$$\begin{aligned}&L_t\frac{\mathrm{d}G_1}{\mathrm{d}t}+\frac{1}{2}f_0(2-b_0)\frac{G_0G_1}{\rho^*}\left[\frac{L_t}{D}+\sum_{j=1}K_j\right]\\&=\rho^* g\beta\oint T_1(t,s)\underline{e}_z\cdot\underline{e}_s(s)\,\mathrm{d}s,\end{aligned} \tag{20}$$

$$\rho^* c_p\frac{\partial T_1}{\partial t}+G_0c_p\frac{\partial T_1}{\partial s}+G_1c_p\frac{\mathrm{d}T_0}{\mathrm{d}s}=\begin{cases}-\overline{h}T_1\dfrac{P}{A} & \text{cooler}\\ 0 & \text{heater}\\ 0 & \text{otherwise}\end{cases}. \tag{21}$$

Due to the invariance of the equations regarding time translations, the following form for the perturbations is proposed: $\theta_1(s,t)=\widehat{\theta}(s)\exp(\omega t)$, where $\omega\in\mathbb{C}$ and θ_1 can be any field such as G_1 or T_1. Besides eliminating the partial derivatives, the Fourier transform has the advantage of providing a simple stability condition for the perturbation, which states that the real part of ω must be negative: $\Re(\omega)<0$.

It is more convenient to work with dimensionless variables. Hence, the following variable changes are adopted:

$$\begin{aligned}&\overline{\omega}\doteq\omega L_t\rho^*/G_0,\quad \overline{G}\doteq\widehat{G}/G_0,\quad \overline{T}\doteq\widehat{T}/\Delta T_0,\\&\overline{s}\doteq s/L_t,\quad \overline{\varphi}\doteq\varphi L_t,\quad \overline{L}_i\doteq L_i/L_t.\end{aligned} \tag{22}$$

It is important to note that the dimensionless variable $\overline{\omega}$ is scaled using the time needed for the flow to complete a full turn around the circuit. When adopting the former variable changes, the dimensionless linear equations are

$$\begin{aligned}&\overline{\omega}\overline{G}+\frac{1}{2}f_0\left[\frac{L_t}{D}+\sum_{j=1}K_j\right]\Bigg[(2-b_0)\overline{G}\\&\quad-\frac{L_t}{\alpha\mathcal{L}_{heater}+(1-\alpha)\mathcal{L}_{int}}\oint\overline{T}(\overline{s})\underline{e}_z\cdot\underline{e}_s(\overline{s})\,\mathrm{d}\overline{s}\Bigg]=0,\end{aligned} \tag{23}$$

$$\frac{\mathrm{d}\overline{T}}{\mathrm{d}\overline{s}}+\overline{\omega}\overline{T}+\overline{G}\frac{1}{\Delta T_0}\frac{\mathrm{d}T_0}{\mathrm{d}\overline{s}}=\begin{cases}-\overline{\varphi}\overline{T} & \text{cooler}\\ 0 & \text{heater}\\ 0 & \text{otherwise}\end{cases}, \tag{24}$$

where $f_0\doteq f(Re_0)$ is the steady state friction factor.

[3] The dependence of a and b on the time varying $G_1(t)$ is not considered when obtaining the linear momentum equation. This approximation only introduces an error inside the laminar-turbulent transition zone. Outside the transition zone shown in Fig. 2, a and b are almost constant. Hence, the above approximation is valid in the far laminar and turbulent regions.

Since a friction factor with continuous derivative is adopted, the momentum equation will vary smoothly when transitioning between the laminar and turbulent regimes.

Even though the heat transfer coefficient $\overline{h}$ may have a dependence on Re (especially in turbulent conditions), the variation of $\overline{h}$ due to the perturbation G_1 is neglected in this work. A preliminary investigation in this direction has been carried out by Pini et al. (2014).

As noted, the momentum Eq. (23) is expressed as function of the stationary Reynolds number Re_0. However, it can be also written in terms of the modified Grashof number Gr_m. This last form can be easily written using Eq. (16). Even though the Grashof number describes the amount of natural circulation inside the closed loop, it was chosen to express the Eq. (23) in terms of Re_0 rather than in terms of Gr_m, since Re_0 gives a clearer idea of the flow conditions (laminar, turbulent) inside the circuit. This will be useful in order to identify the flow regime transitions in the stability maps.

2.2.1. Calculation of the temperature perturbation

Eq. (24) is solved for all the sections inside the closed-loop. The temperature perturbation inside the cooler is given by

$$\overline{T}(\overline{s}) = \overline{T}(\overline{s}=0)\exp(-(\overline{\omega}+\overline{\varphi})\overline{s}) + \frac{\overline{G}\overline{\varphi}}{\overline{\omega}}\frac{1}{1-\exp(-\overline{\varphi}\overline{L}_c)} \times [\exp(-\overline{\varphi}\overline{s}) - \exp(-(\overline{\omega}+\overline{\varphi})\overline{s})]. \tag{25}$$

The temperature perturbation distribution inside the cold leg is

$$\overline{T}(\overline{s}) = \overline{T}(\overline{L}_c)\exp\left(-\overline{\omega}(\overline{s}-\overline{L}_c)\right) - \frac{\overline{G}}{\overline{\omega}}\frac{1-\alpha}{1-\overline{L}_c}\times\left[1-\exp\left(-\overline{\omega}(\overline{s}-\overline{L}_c)\right)\right], \tag{26}$$

where $\overline{T}(\overline{L}_c)$ is the temperature perturbation at the cooler exit. The temperature perturbation $\overline{T}(\overline{s})$ inside the circuit heater is

$$\overline{T}(\overline{s}) = \overline{T}(\overline{L}_c+\overline{L}_{cl})\exp\left(-\overline{\omega}[\overline{s}-(\overline{L}_c+\overline{L}_{cl})]\right) - \frac{\overline{G}}{\overline{\omega}}\left[\frac{\alpha}{\overline{L}_h}+\frac{1-\alpha}{1-\overline{L}_c}\right]\left[1-\exp\left(-\overline{\omega}[\overline{s}-(\overline{L}_c+\overline{L}_{cl})]\right)\right], \tag{27}$$

where $\overline{T}(\overline{L}_c+\overline{L}_{cl})$ is the temperature perturbation at the cold leg exit. Finally, the perturbed temperature distribution inside the hot leg is

$$\overline{T}(\overline{s}) = \overline{T}(\overline{L}_c+\overline{L}_{cl}+\overline{L}_h)\exp\left(-\overline{\omega}[\overline{s}-(\overline{L}_c+\overline{L}_{cl}+\overline{L}_h)]\right) - \frac{\overline{G}}{\overline{\omega}}\frac{1-\alpha}{1-\overline{L}_c}\left[1-\exp\left(-\overline{\omega}[\overline{s}-(\overline{L}_c+\overline{L}_{cl}+\overline{L}_h)]\right)\right], \tag{28}$$

where $\overline{T}(\overline{L}_c+\overline{L}_{cl}+\overline{L}_h)$ is the temperature perturbation at the heater exit.

The temperature perturbation $\overline{T}(\overline{s})$ after one circuit loop must also be continuous at $\overline{s}=0$. Hence, the boundary condition for the temperature perturbation, $\overline{T}(\overline{s}=0)=\overline{T}(\overline{s}=1)$, gives the following relation:

$$\overline{T}(0) = \frac{\overline{T}(1)-\overline{T}(0)\exp\left(-(\overline{\omega}+\overline{\varphi}\overline{L}_c)\right)}{1-\exp\left(-(\overline{\omega}+\overline{\varphi}\overline{L}_c)\right)}, \tag{29}$$

where $\overline{T}(1)$ is the temperature perturbation at the hot leg exit and is given by Eq. (28). Since Eqs. (20) and (21) are linear, the temperature perturbation $\overline{T}(\overline{s})$ depends linearly on the perturbation mass flux $\overline{G}$. It is simple to verify that the numerator in Eq. (29) does not depend on $\overline{T}(0)$ and that it is proportional to $\overline{G}$.

2.2.2. Dispersion relation

In order to find the dispersion relation for $\overline{\omega}$, the conservation Eq. (23) is used. Since it is known that $\overline{T} \propto \overline{G}$ from Eq. (29), the line integral in Eq. (23) can be written as

$$\overline{G}\mathcal{A}(\overline{\omega},\overline{\varphi},\alpha) \doteq \oint \overline{T}(\overline{s})\underline{e}_z\cdot\underline{e}_s(\overline{s})\,\mathrm{d}\overline{s} = \int_{up}\overline{T}(\overline{s})\,\mathrm{d}\overline{s} - \int_{down}\overline{T}(\overline{s})\,\mathrm{d}\overline{s}, \tag{30}$$

where $\mathcal{A}(\overline{\omega},\overline{\varphi},\alpha)$ is a function that does not depend on $\overline{G}$, $\int_{down}$ is the line integral of the temperature perturbation taken along the loop sections in which the fluid is falling and $\int_{up}$ is the line integral taken along the sections in which the fluid is rising. Using the temperature perturbation given by Eqs. (25)–(28), these integrals are later calculated for several circuit configurations (see Section 3). When inserting the defined function $\mathcal{A}(\overline{\omega},\overline{\varphi},\alpha)$ in Eq. (23), the dispersion relation for $\overline{\omega}$ is

$$\overline{\omega}+\frac{1}{2}f_0\left[\frac{L_t}{D}+\sum_{j=1}K_j\right]\left[(2-b_0)-\frac{L_t\mathcal{A}(\overline{\omega},\overline{\varphi},\alpha)}{\alpha\mathcal{L}_{heater}+(1-\alpha)\mathcal{L}_{int}}\right]=0. \tag{31}$$

As shown, the dispersion relation depends on the steady-state Reynolds number Re_0 (acting through f_0 and b_0), the modified Stanton number (proportional to $\overline{\varphi}$), the flow direction, the parameter α, and the system geometry. From the dispersion relation (31), the stability maps for different closed loop circuits will be constructed in which the free parameters are Re_0, St_m, and α.

2.3. Numerical nonlinear stability analysis

The linear analysis method is a powerful mathematical tool that allows determining the stability behavior of a convective natural circulation system. During the process of making the Eqs. (1)–(3) linear, second-order terms were neglected. This approximation is convenient when the perturbations are consid-ered small. For larger perturbations, numeric codes are usually implemented in order to solve the nonlinear time-independent Eqs. (1)–(3). In the present work, the numerical nonlinear analysis is simply used to confirm the results given by the linear stability analysis.

The goal is to numerically calculate the temporal evolution of the flow flux $G(t)$ and the temperature distribution $T(s,t)$ when a perturbation is given around the stationary state of the system. It is considered that the mass flux and the temperature distribution have the form

$$G(t) = G_0 + G_1(t),\qquad T(s,t) = T_0(s) + T_1(s,t). \tag{32}$$

When inserting these variables into Eqs. (1)–(3) and using the variable changes presented in Eq. (22) together with the dimensionless time variable $\overline{t} = tG_0/(L_t\rho^*)$, the following nonlinear equations are obtained:

$$\frac{\mathrm{d}\overline{G}}{\mathrm{d}\overline{t}} = \frac{1}{2}f_0\left[\frac{L_t}{D}+\sum_{j=1}K_j\right]\left[1-\frac{f}{f_0}(1+\overline{G})^2 + \frac{L_t}{\alpha\mathcal{L}_{heater}+(1-\alpha)\mathcal{L}_{int}}\oint\overline{T}(\overline{s},\overline{t})\underline{e}_z\cdot\underline{e}_s(\overline{s})\,\mathrm{d}\overline{s}\right], \tag{33}$$

$$\frac{\partial\overline{T}}{\partial\overline{t}} + (1+\overline{G})\frac{\partial\overline{T}}{\partial\overline{s}} + \frac{\overline{G}}{\Delta T_0}\frac{\mathrm{d}T_0}{\mathrm{d}\overline{s}} = \begin{cases} -\overline{\varphi}\overline{T} & \text{cooler} \\ 0 & \text{heater} \\ 0 & \text{otherwise} \end{cases}. \tag{34}$$

There are several aspects in Eq. (33) that should be noted. Here, $f_0 = f(G_0)$ denotes the friction coefficient calculated in the stationary state while $f = f(G_0+G_1)$ denotes the friction coefficient when the perturbation is present. It must be noted that a key difference between the momentum conservation eqs. (23) and (33) is that the dependence of the friction factor coefficients, a and b, with $G_1(t)$ is considered. In the linear analysis, these variations are neglected because the variations of a and b are negligible outside the flow regime transition zone. Hence, it is expected that the stability maps generated by the linear and nonlinear formulations will show differences in the laminar-turbulent transition zone (Section 4.1).

In this work, Eqs. (33) and (34) are discretized using a *MacCormack Scheme* (MacCormack, 1969). This scheme has been used previously to calculate the stability maps of natural circulating systems (Ambrosini and Ferreri, 1998, 2000). The numerical simulations were performed in a MATLAB (2013) environment.

3. Stability analysis on rectangular loops of circular cross section

In this section, the general stability analysis methods of Section 2 are applied to study the dynamical stability of different configurations of rectangular closed loops. Two circuit configurations are analyzed. The first circuit is the Vertical Heater – Horizontal Cooler (VHHC) circuit. In this loop, the heater is placed in a vertical position while the cooler is placed in an horizontal position above the heater. The second analyzed circuit is the Vertical Heater – Vertical Cooler (VHVC) circuit. Both heater and cooler are placed in vertical positions in different legs. These configurations will be analyzed separately.

3.1. Vertical heater–horizontal cooler (VHHC) loop

Fig. 4 shows a diagram of the VHHC system with a clock-wise fluid circulation. Following the notation presented in Section 2.1, the origin of the curvilinear coordinate, s, is located at the cooler entrance. The length of the cold leg is $L_{cl}=L_1+L_2+L_3+L_4$, while the length of the hot leg is $L_{hl}=L_5+L_6$.

The stationary state of the system is calculated from Eq. (12). The line integral of the steady state temperature field must be calculated:

$$\oint T_0(s)\underline{e}_z\cdot\underline{e}_s(s)\,\mathrm{d}s=\int_{\langle L_4+L_h+L_5\rangle}T_0(s)\,\mathrm{d}s-\int_{\langle L_2\rangle}T_0(s)\,\mathrm{d}s, \tag{35}$$

where the notation $\langle\cdot\rangle$ denotes the circuit segments in which the integration must be made. After evaluating of the line integral, a relation between the steady state fields, G_0 and ΔT_0, is obtained:

$$\frac{1}{2}f_0\frac{G_0^2}{\rho^*}\left[\frac{L_t}{D}+\sum_{j=1}K_j\right]=\rho^*\beta g\Delta T_0\left[\alpha\left(L_5+\frac{L_h}{2}\right)+(1-\alpha)L_2\frac{L_2+L_3}{L_t-L_c}\right]. \tag{36}$$

From Eq. (36), it is now possible to identify the variables, $\mathcal{L}_{heater}=L_5+L_h/2$ and $\mathcal{L}_{int}=(L_2)(L_2+L_3)/(L_t-L_c)$, which were introduced in Eqs. (13) and (15). $\mathcal{L}_{heater}$ and $\mathcal{L}_{int}$ have a physical meaning. $\mathcal{L}_{heater}$ represents the height difference between the thermal barycenters of the heater and the cooler. The interpretation for $\mathcal{L}_{int}$ is more complicated, namely the ratio $(L_2+L_3)/(L_t-L_c)$ shows that the effective convective force given by the internal heat generation comes from the heat generated inside segments L_2 and L_3; the contribution in temperature change by segments L_2 and L_3 is then multiplied by L_2, which is the circuit total height.

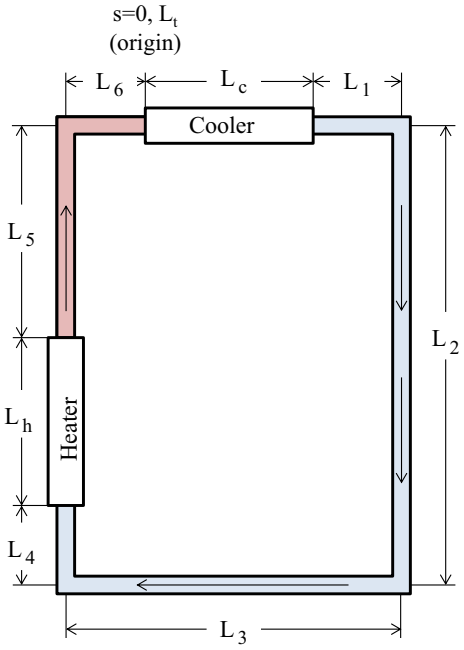

Fig. 4. Schema of the VHHC system.

In order to proceed with the linear stability analysis, the procedure described in Section 2.2 is followed. The line integral of the temperature perturbation field given in Eqs. (30) and (31) needs to be calculated:

$$\overline{G}\mathcal{A}_{VHHC}\doteq\oint\overline{T}(\bar{s})\underline{e}_z\cdot\underline{e}_s(\bar{s})\,\mathrm{d}\bar{s}=\int_{up}\overline{T}(\bar{s})\,\mathrm{d}\bar{s}-\int_{down}\overline{T}(\bar{s})\,\mathrm{d}\bar{s}. \tag{37}$$

Using the calculated expressions for the temperature perturbation, Eqs. (25)–(28), the line integrals are

$$\begin{aligned}\int_{up}\overline{T}(\bar{s})\,\mathrm{d}\bar{s}&=\int_{\langle\bar{L}_4+\bar{L}_h+\bar{L}_5\rangle}\overline{T}(\bar{s})\,\mathrm{d}\bar{s}\\&=-\overline{T}(\bar{L}_c)\frac{1}{\overline{\omega}}\left[e^{-\overline{\omega}\bar{L}_{cl}}-e^{-\overline{\omega}(\bar{L}_1+\bar{L}_2+\bar{L}_3)}\right]\\&\quad-\frac{\overline{G}}{\overline{\omega}}\frac{1-\alpha}{1-\bar{L}_c}\left[\bar{L}_4+\frac{1}{\overline{\omega}}\left(e^{-\overline{\omega}\bar{L}_{cl}}-e^{-\overline{\omega}(\bar{L}_1+\bar{L}_2+\bar{L}_3)}\right)\right]\\&\quad-\overline{T}(\bar{L}_c+\bar{L}_{cl})\frac{1}{\overline{\omega}}\left[e^{-\overline{\omega}\bar{L}_h}-1\right]\\&\quad-\frac{\overline{G}}{\overline{\omega}}\left[\frac{\alpha}{\bar{L}_h}+\frac{1-\alpha}{1-\bar{L}_c}\right]\left[\bar{L}_h+\frac{1}{\overline{\omega}}\left(e^{-\overline{\omega}\bar{L}_h}-1\right)\right]\\&\quad-\overline{T}(\bar{L}_c+\bar{L}_{cl}+\bar{L}_h)\frac{1}{\overline{\omega}}\left[e^{-\overline{\omega}\bar{L}_5}-1\right]\\&\quad-\frac{\overline{G}}{\overline{\omega}}\frac{1-\alpha}{1-\bar{L}_c}\left[\bar{L}_5+\frac{1}{\overline{\omega}}\left(e^{-\overline{\omega}\bar{L}_5}-1\right)\right],\end{aligned} \tag{38}$$

$$\begin{aligned}\int_{down}\overline{T}(\bar{s})\,\mathrm{d}\bar{s}&=\int_{\langle\bar{L}_2\rangle}\overline{T}(\bar{s})\,\mathrm{d}\bar{s}\\&=-\overline{T}(\bar{L}_c)\frac{1}{\overline{\omega}}\left[e^{-\overline{\omega}(\bar{L}_2+\bar{L}_1)}-e^{-\overline{\omega}\bar{L}_1}\right]\\&\quad-\frac{\overline{G}}{\overline{\omega}}\frac{1-\alpha}{1-\bar{L}_c}\left[\bar{L}_2+\frac{1}{\overline{\omega}}\left(e^{-\overline{\omega}(\bar{L}_1+\bar{L}_2)}-e^{-\overline{\omega}\bar{L}_1}\right)\right].\end{aligned} \tag{39}$$

Eqs. (37)–(39) together with Eq. (29) and the dispersion relation (31) form a closed system of equations for which $\overline{\omega}$ can be solved as function of the flow parameters: Re, St_m, and α.

3.2. Vertical heater–vertical cooler (VHVC) loop

This type of circuit is of special importance because it exemplifies better the current dominating designs for natural circulating systems in the nuclear industry (IAEA, 2005). In the following analysis, the circulation of the fluid is considered clockwise because this motion is known to be more stable (Wu and Sienicki, 2003). Following the notation of Section 2.1, the origin of the coordinate s is located at the cooler entrance. The length of the cold leg is given by $L_{cl}=L_1+L_2+L_3$, while the length of the hot leg is written as $L_{hl}=L_4+L_5+L_6$.

As done previously for the VHHC system, the steady state of the VHVC system must be determined first. The line integral of the steady state temperature field $T_0(s)$ in Eq. (12) is calculated:

$$\oint T_0(s)\underline{e}_z\cdot\underline{e}_s(s)\,\mathrm{d}s=\int_{\langle L_3+L_h+L_4\rangle}T_0(s)\,\mathrm{d}s-\int_{\langle L_6+L_c+L_1\rangle}T_0(s)\,\mathrm{d}s. \tag{40}$$

By using the general steady state temperature distribution (9), the expressions for $\mathcal{L}_{heater}$ and $\mathcal{L}_{int}$ are obtained:

$$\mathcal{L}_{heater} = \frac{L_h}{2} + L_4 - L_6 + \frac{L_c}{e^{\varphi L_c} - 1} - \frac{1}{\varphi},$$

$$\mathcal{L}_{int} = H\frac{L_1 + L_2}{L_t - L_c} - L_6\frac{L_t - L_c - L_6}{L_t - L_c} + \frac{1}{2}\frac{H^2 - L_6^2 - L_1^2}{L_t - L_c} + \frac{L_c}{e^{\varphi L_c} - 1} - \frac{1}{\varphi}. \tag{41}$$

Here, we have defined $H \doteq L_3 + L_h + L_4$ is the height of the circuit (see Fig. 5). As it can be seen, the expressions for $\mathcal{L}_{heater}$ and $\mathcal{L}_{int}$ are more complicated than those calculated previously for the VHHC circuit. However, it can be still seen that $\mathcal{L}_{heater}$ always represents the height difference between the heater and cooler thermal barycenters. The terms in $\mathcal{L}_{int}$ are more complicated to interpret.

In order to continue with the linear stability analysis, the procedure described in Section 2.2 is followed. The line integral of the temperature perturbation $\overline{T}(\overline{s})$ in Eqs. (30) and (31) needs to be calculated. Evaluation of the line integral gives

$$\overline{G}\mathcal{A}_{VHVC} \doteq \oint \overline{T}(\overline{s})\underline{e}_z \cdot \underline{e}_s(\overline{s})\,\mathrm{d}\overline{s} = \int_{up} \overline{T}(\overline{s})\,\mathrm{d}\overline{s} - \int_{down} \overline{T}(\overline{s})\,\mathrm{d}\overline{s}, \tag{42}$$

where

$$\begin{aligned}
\int_{up} \overline{T}(\overline{s})\,\mathrm{d}\overline{s} &= \int_{\langle \overline{L}_3 + \overline{L}_h + \overline{L}_4 \rangle} \overline{T}(\overline{s})\,\mathrm{d}\overline{s} \\
&= -\overline{T}(\overline{L}_c)\frac{1}{\overline{\omega}}\left[e^{-\overline{\omega}\overline{L}_{cl}} - e^{-\overline{\omega}(\overline{L}_1 + \overline{L}_2)}\right] \\
&\quad -\frac{\overline{G}}{\overline{\omega}}\frac{1-\alpha}{1-\overline{L}_c}\left[\overline{L}_3 + \frac{1}{\overline{\omega}}\left(e^{-\overline{\omega}\overline{L}_{cl}} - e^{-\overline{\omega}(\overline{L}_1 + \overline{L}_2)}\right)\right] \\
&\quad -\overline{T}(\overline{L}_c + \overline{L}_{cl})\frac{1}{\overline{\omega}}\left[e^{-\overline{\omega}\overline{L}_h} - 1\right] \\
&\quad -\frac{\overline{G}}{\overline{\omega}}\left[\frac{\alpha}{\overline{L}_h} + \frac{1-\alpha}{1-\overline{L}_c}\right]\left[\overline{L}_h + \frac{1}{\overline{\omega}}\left(e^{-\overline{\omega}\overline{L}_h} - 1\right)\right] \\
&\quad -\overline{T}(\overline{L}_c + \overline{L}_{cl} + \overline{L}_h)\frac{1}{\overline{\omega}}\left[e^{-\overline{\omega}\overline{L}_4} - 1\right] \\
&\quad -\frac{\overline{G}}{\overline{\omega}}\frac{1-\alpha}{1-\overline{L}_c}\left[\overline{L}_4 + \frac{1}{\overline{\omega}}\left(e^{-\overline{\omega}\overline{L}_4} - 1\right)\right],
\end{aligned} \tag{43}$$

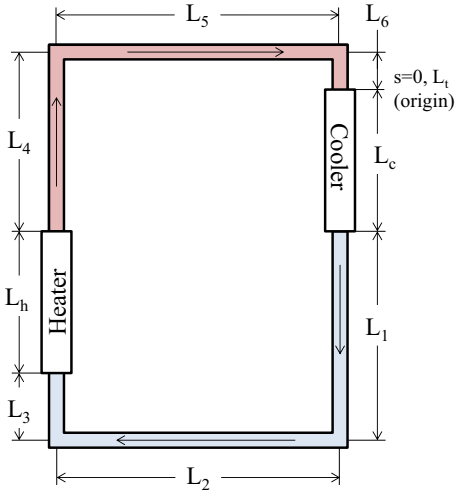

Fig. 5. Schema of the VHVC system.

$$\begin{aligned}
\int_{down} \overline{T}(\overline{s})\,\mathrm{d}\overline{s} &= \int_{\langle \overline{L}_6 + \overline{L}_c + \overline{L}_1 \rangle} \overline{T}(\overline{s})\,\mathrm{d}\overline{s} \\
&= -\overline{T}(\overline{L}_c + \overline{L}_{cl} + \overline{L}_h)\frac{1}{\overline{\omega}}\left[e^{-\overline{\omega}\overline{L}_{hl}} - e^{-\overline{\omega}(\overline{L}_{hl} - \overline{L}_6)}\right] \\
&\quad -\frac{\overline{G}}{\overline{\omega}}\frac{1-\alpha}{1-\overline{L}_c}\left[\overline{L}_6 + \frac{1}{\overline{\omega}}\left(e^{-\overline{\omega}\overline{L}_{hl}} - e^{-\overline{\omega}(\overline{L}_{hl} - \overline{L}_6)}\right)\right] \\
&\quad -\overline{T}(0)\frac{1}{\overline{\omega} + \overline{\varphi}}\left[e^{-(\overline{\omega} + \overline{\varphi})\overline{L}_c} - 1\right] \\
&\quad +\frac{\overline{G}\overline{\varphi}}{\overline{\omega}}\frac{1}{1 - \exp(-\overline{\varphi}\overline{L}_c)}\left[-\frac{1}{\overline{\varphi}}\left[e^{-\overline{\varphi}\overline{L}_c} - 1\right]\right. \\
&\quad \left.+\frac{1}{\overline{\omega} + \overline{\varphi}}\left(e^{-(\overline{\varphi} + \overline{\omega})\overline{L}_c} - 1\right)\right] \\
&\quad -\overline{T}(\overline{L}_c)\frac{1}{\overline{\omega}}\left[e^{-\overline{\omega}\overline{L}_1} - 1\right] \\
&\quad -\frac{\overline{G}}{\overline{\omega}}\frac{1-\alpha}{1-\overline{L}_c}\left[\overline{L}_1 + \frac{1}{\overline{\omega}}\left(e^{-\overline{\omega}\overline{L}_1} - 1\right)\right].
\end{aligned} \tag{44}$$

Here, the line integrals were calculated using Eqs. (25)–(28) for the temperature perturbation. Eqs. (29) and (42)–(44) are inserted into Eq. (31) in order to determine $\overline{\omega}$ as function of the flow parameters: Re, St_m, and α.

4. Results and discussion

4.1. Vertical heater–horizontal cooler (VHHC) loop

Before presenting the main results, the developed codes of this work are verified. For the verification process, the generated stability maps of this work are compared with those previously published by other authors in which no internal heat generation was considered. Table 1 presents the dimensions of the VHHC circuit that was used. The VHHC circuit has the same dimensions of the VHHC loop studied in a previous work by Vijayan et al. (2007). The same geometry is used in order to compare our results in the case where no internal heat generation ($\alpha = 1$) is present.

Before discussing the obtained stability maps, it is worth mentioning the procedure used to calculate the stability maps. The stability maps plot the curve $Re = Re(St_m)$ that shows the boundary between the unstable and stable operating regimes. This curve is obtained by solving Eqs. (29), (31), and (37)–(39). First, the operating parameters Re and α are specified. In order to obtain the stability boundary, we force $\Re\{\overline{\omega}\} = 0$. Then, the real and imaginary components of Eq. (31) are solved in order to obtain St_m and $\Im\{\overline{\omega}\}$. In this work, the *Trust-Region-Dogleg* algorithm of MATLAB (2013) was used to solve the system of equations.

In Fig. 6, the stability map of the VHHC circuit with no internal heat generation ($\alpha = 1$) generated by our code is compared with previously published stability maps (Vijayan et al., 2007). In this mentioned work, the stability maps for laminar and turbulent regimes are presented separately by having the friction factor function held fixed. Fig. 6 compares the generated stability maps using the same laminar and turbulent friction correlations. As shown, the previous results are replicated by our code.

Fig. 7 presents the generated stability maps with the friction factor given in Eq. (5). As shown, the generated stability maps correctly match the previous results for low and high Grashof

Table 1
Dimensions of the VHHC and VHVC circuits studied.

Circuit	L_1 (m)	L_2 (m)	L_3 (m)	L_4 (m)	L_5 (m)	L_6 (m)	L_c (m)	L_h (m)	H (m)	L_t (m)	D (m)
VHHC	0.31	2.20	1.42	0.35	1.12	0.31	0.80	0.73	2.20	7.24	0.0269
VHVC (I)	1.18	1.42	0.35	1.12	1.42	0.22	0.80	0.73	2.20	7.24	0.0269
VHVC (II)	1.40	1.42	0.00	1.47	1.42	0.00	0.80	0.73	2.20	7.24	0.0269

numbers, where the fluid flow is surely in a full laminar or turbulent regime. However, differences in the stability maps appear around $Gr_m \sim 10^{11}$. This difference is due to the transition region of the friction factor (see Fig. 2). These results show that the choice of the friction factor has a strong impact on the shape of the stability maps near the transition region.

For further verification, the stability map generated by the linear method is compared to that generated by the numerical nonlinear method. In order to generate the stability maps using the nonlinear formulation, Eqs. (33) and (34) are numerically solved for given Re, St_m, and α. For a small positive initial perturbation on the mass flux density, $\overline{G}(t)$ is evolved in time. Fig. 8 shows typical examples of the temporal evolution of the mass flux perturbation. The simulation parameters used are shown in Fig. 9. In order to determine if the flow is stable, the logarithmic growth rate of the oscillation maxima is calculated. If the logarithmic growth rate is larger than a certain tolerance level, the flow is considered unstable. Simulations are made for fixed Re and α while iterating the St_m until the flow regime is stable. Once the St_m parameter is obtained for stable flow, the Reynolds number is iterated, and the process is repeated again until the whole stability map is calculated.

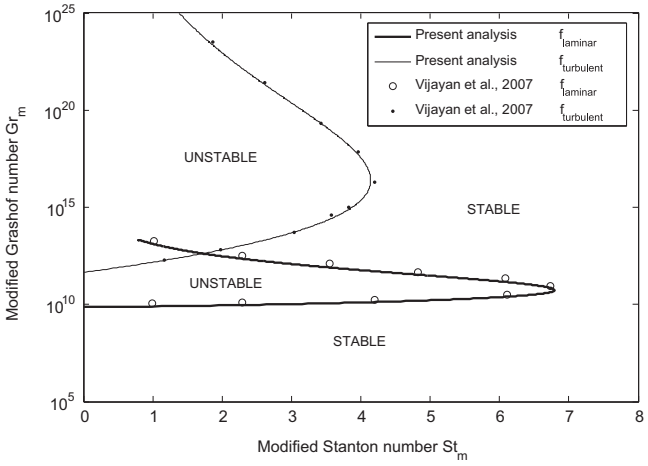

Fig. 6. Stability maps of the VHHC circuit with no internal heat generation ($\alpha = 1$). The curves are calculated using fixed friction factors. The results are compared with previously published results (Vijayan et al., 2007).

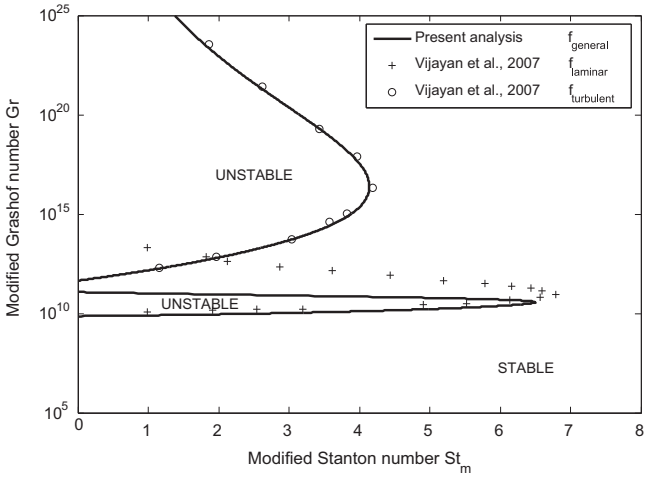

Fig. 7. Stability maps of the VHHC circuit with no internal heat generation ($\alpha = 1$). Using the friction factor of Eq. (5), the generated stability maps are compared with previously published results (Vijayan et al., 2007).

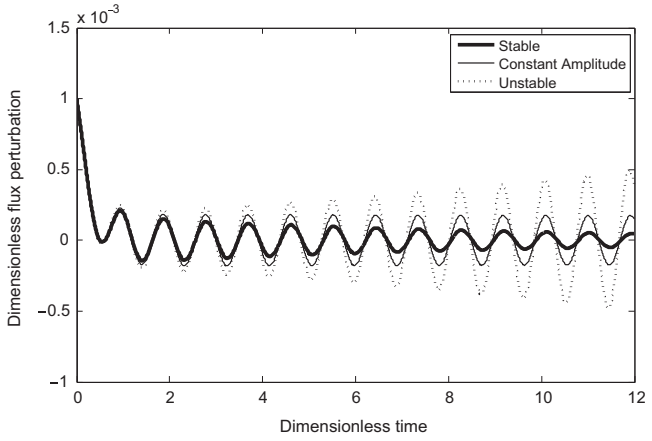

Fig. 8. Time evolution of perturbed mass flux $\overline{G}$. Examples of stable, unstable and constant mass flux oscillations are shown. The simulation parameters used are denoted with "+" in the stability map of Fig. 9.

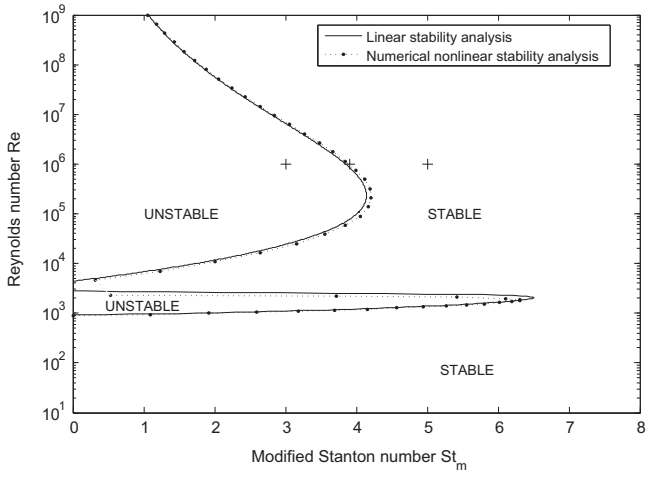

Fig. 9. Stability maps for the VHHC loop with no internal heat generation ($\alpha = 1$). The maps calculated by the linear and numerical nonlinear methods show good agreement. The physical parameters used for the simulations presented in Fig. 8 are shown with the symbol "+" in the stability map.

Fig. 9 compares the stability maps using the linear and nonlinear analysis methods. As it can be seen, the two approaches show good agreement. Since the two approaches are independent, this result validates, in a certain sense, the methods and codes developed in this work.

As mentioned in the Introduction, internal heat generation can affect significantly the stability maps of natural circulating loops. Fig. 10 shows the stability maps of the VHHC circuit for different levels of internal heat generation. The stability maps shown correspond to $\alpha = 1$ (only external heating), $\alpha = 0.5$, $\alpha = 0.3$, and $\alpha = 0$ (only internal heat generation). As shown, the unstable zone increases steadily when the portion of power coming from internal heat generation increases, $\alpha \to 0$. The increase of the instability zone might be explained as follows: when $\alpha = 1$, the fluid preferably flows in the clockwise direction. When $\alpha = 0$ (no heater), the situation is different. In this case, the loop has left-right symmetry with the cooler located in the top center part of the circuit. The fluid does not have any preferable flowing direction. The lack of any preferable flow direction could be the cause of the large increase of the instability zone at low Re. However, the

effect is less noticeable at high *Re*. These findings suggest that the effects of internal heat generation on natural circulation stability should be considered when designing internally heated loops.

To further verify this result, the stability maps with only internal heat generation ($\alpha = 0$) generated by the linear analysis and the numerical nonlinear method are compared. Fig. 11 presents both stability maps. As it can be seen, there is an overall good agreement between the stability maps. However, at $Re \sim 2500$ differences appear between the linear and nonlinear stability maps. This is caused by the transition zone of the friction factor. In the linear analysis, Eq. (20) ignores the dependence of the friction correlation a and b factors on the flux perturbation G_1. On the other hand, the nonlinear numerical analysis does not use this approximation and thus predicts a slight gain of stability. The gain in instability is due to the minimum in the friction factor at the transition zone. Nevertheless, the results of the linear stability analysis should not be undermined because of the error seen in the transition zone. In reality, the transition zone is not very well understood, and most engineers try to avoid operating in this region.

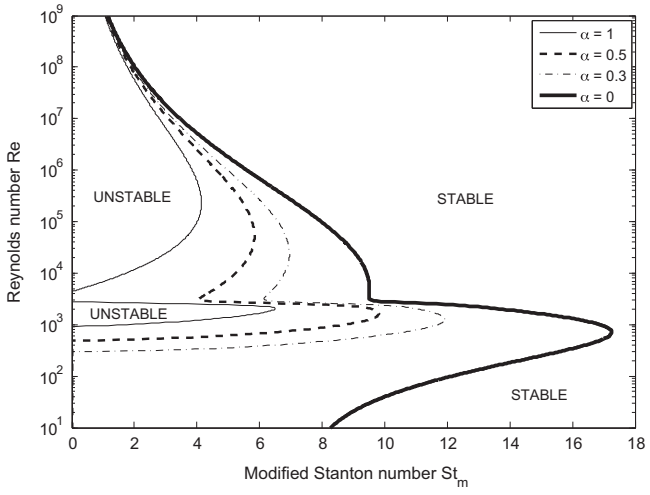

Fig. 10. Stability maps for a VHHC system for various levels of internal heat generation. The instability zone grows as the internal heat generation becomes more dominant.

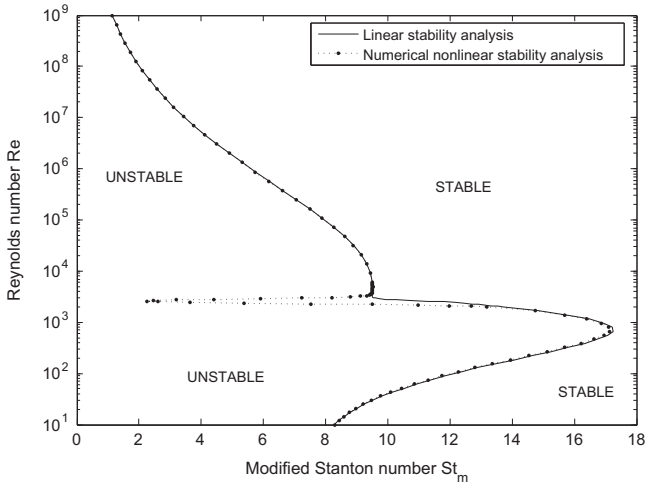

Fig. 11. Stability maps for the VHHC loop with internal heat generation only ($\alpha = 0$). The maps calculated by the linear and numerical nonlinear methods show good agreement except in the transition region. The differences arise due to the strong nonlinear behavior of the friction factor at the transition zone.

4.2. Vertical heater–vertical cooler (VHVC) loop

The dimensions of the analyzed VHVC circuits are presented in Table 1. Notice that the geometries of the VHVC circuits are very similar to that of the VHHC circuit analyzed previously. Both loops have the same total length L_t, the same vertical height H, and the same tube diameter D. In fact, only the placement of the cooler inside the loop is modified with respect to the VHHC loop previously studied. The similar characteristics between the circuits will allow us to compare their stability maps.

Fig. 12 presents the stability maps for the VHVC (I) and VHVC (II) circuits with parameters: $\alpha = 1$ (only external heating), $\alpha = 0.5$, and $\alpha = 0$ (only internal heat generation). The first feature that can be noticed is that the unstable region for the VHVC circuits is significantly smaller than the one of the VHHC circuit analyzed earlier (see Fig. 10). When internal heat generation is present, the unstable zone also grows but does not increase as much as in the case of the VHHC circuit. A possible reason why the unstable zone grows slower might be that the VHVC loop still remains asymmetric even when the external heater is removed from the circuit ($\alpha = 0$). The asymmetry due to the position of the cooler brings more stability to the system. The more stable behavior shown by the VHVC circuit makes this circuit configuration interesting for engineering applications.

The effects due to the height difference between the cooler and heater thermal barycenters were also investigated. In the VHVC (II) loop, the cooler was raised 22 cm while the heater was lowered 35 cm with respect to the configuration of the VHVC (I) loop. Hence, the overall geometry of the two circuits is the same; however, the thermal barycenter height difference between the heater and cooler is larger for the VHVC (II) loop. Fig. 12 shows the variation of the stability maps for $\alpha = 1$, $\alpha = 0.5$, and $\alpha = 0$. As shown, the instability zone decreases for all α when the vertical height difference between the heater and cooler is smaller. Even though the instability zone is smaller for the VHVC (I) loop, the drawback of this loop is that the convective driving force is also smaller (Welander, 1967). From an engineering point of view, a good natural circulation loop will be the one that guarantees a sufficient mass flux for the envisioned applications while avoiding as much as possible the unstable operating modes. To perform such analysis, it is also required to solve the steady state Eqs. (9)–(12) with the appropriate equations of state for the fluid parameters (ρ_0, β, μ) to map the steady-state operating curves on the stability maps. This endeavor was not pursued in this work.

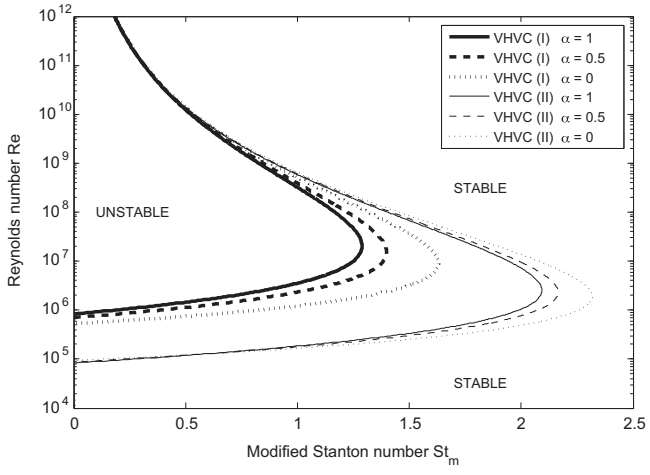

Fig. 12. Stability maps for a VHVC system for various levels of internal heat generation. The instability zone does not show an important growth as the internal heat generation becomes dominant.

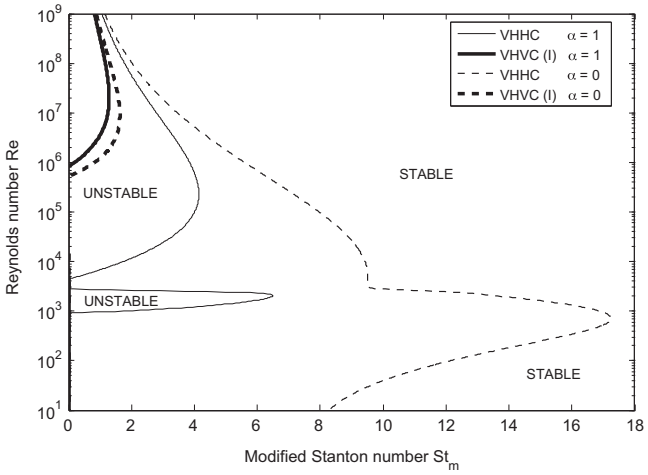

Fig. 13. Comparison of the stability maps of the VHHC and VHVC (I) circuit loops. The VHVC (I) configuration shows a better behavior regarding stability for different levels on internal heat generation.

5. Conclusions

In this work, the effects of internal heat generation on the stability of natural circulation closed-loop systems are investigated. Two methods are used: a linear semianalytical method and a numerical nonlinear method. These methods are applied to study the stability maps of different configuration loops when internal heat generation is present. In this study, it is found that the unstable region of the stability maps increases when the fluid internal heat generation becomes larger. Among the studied configurations, the Vertical Heater - Vertical Cooler (VHVC) circuit loop shows a better behavior regarding stability when internal heat generation is present (see Fig. 13). The unstable region of this circuit is the smallest and has only a small growth when the internal heat generation becomes dominant. These findings suggest that internal heating effects should be taken into consideration when designing internally heated closed-loop convective systems.

For future work, the authors believe that it is fundamental to validate the predictions of the presented model against experimental data. To this purpose, a testing facility (DYNASTY – DYnamics of NAtural circulation for molten SalT internallY heated) is currently being designed at the Politecnico di Milano. It is envisioned that DYNASTY will also provide useful information on 3D effects that were not discussed in this paper, such as: non-uniform power generation, cross-stream temperature gradients effects, and non-uniformity of the fluid parameters. Construction of the facility will begin in the near future.

Nomenclature

Greek symbols

α	parameter describing the ratio between external heating power and the total heating power
β	thermal expansion coefficient (K^{-1})
γ	parameter used in the friction factor
ΔT	temperature difference (K)
μ	dynamic viscosity (Pa s)
ρ	volumetric density (kg m^{-3})
ω	oscillating frequency of the Fourier transform (s^{-1})

Latin symbols

a	coefficient inside the friction factor
A	cross-section area of circuit tube (m^2)
b	coefficient inside the friction factor
c_p	specific heat (J kg^{-1} K^{-1})
D	hydraulic diameter (m)
$\underline{e}_s(s)$	unit vector following the fluid flow
$\underline{e}_z$	unit vector pointing towards the positive vertical direction
f	Darcy friction factor
g	gravitational acceleration (m s^{-1})
$G(t)$	mass flux (kg m^{-2} s^{-1})
Gr	Grashof number $\left(=(\rho^2 g D^3/\mu^2)\beta\Delta T\right)$
Gr_m	modified Grashof number $\left(=(\rho^2 g D^3/\mu^2)\beta\Delta T_m\right)$
$\overline{h}$	heat exchange coefficient (W m^{-2} K^{-1})
$\Im\{\omega\}$	imaginary part of ω
k	thermal conductivity (W m^{-1} K^{-1})
L_i	length of section i of the closed loop (m)
L_t	total length of the closed loop (m)
$\mathcal{L}_{heater}$	geometrical factor describing the contribution of the external heating to the buoyancy force (m)
$\mathcal{L}_{int}$	geometrical factor describing the contribution of the internal heating to the buoyancy force (m)
Nu	Nusselt number $\left(=\overline{h}D/k\right)$
p	pressure (Pa)
P	perimeter of circuit tube (m)
Pr	Prandtl number $(=c_p\mu/k)$
q''	external heat flux (W m^{-2})
q'''	internal heat generation (W m^{-3})
Re	Reynolds number $(=GD/\mu)$
$\Re\{\omega\}$	real part of ω
s	curvilinear coordinate (m)
St	Stanton number $(=Nu\ Re/Pr)$
St_m	modified Stanton number $(=4\ St(L_t/D))$
t	time (s)
$T(s,t)$	fluid temperature (K)
$v(s,t)$	fluid velocity (m s^{-1})

Subscripts and superscripts

0	steady state
1	perturbation
*	reference
c	cooler
cl	cold leg
h	heater
hl	hot leg
int	internal
m	modified
t	total
w	wall

Acronyms

MSR	molten salt reactor
VHHC	vertical heater–horizontal cooler
VHVC	vertical heater–vertical cooler

Acknowledgments

The authors are in particular debt to Alessandro Pini (Politecnico di Milano) and Jacopo de Amicis for fruitful discussions and criticism. The authors gratefully acknowledge the European Nuclear Education Network (ENEN) for supporting part of this work and the FARB (Finanziamenti di Ateneo alla Ricerca di Base) Project for supporting future research on this subject.

References

Ambrosini, W., Ferreri, J., 1998. The effect of truncation error on the numerical prediction of linear stability boundaries in a natural circulation single-phase loop. Nucl. Eng. Des. 183, 53–76.

Ambrosini, W., Ferreri, J., 2000. Stability analysis of single-phase thermosyphon loops by finite-difference numerical methods. Nucl. Eng. Des. 201, 11–23.

Chen, K., 1985. On the oscillatory instability of closed-loop thermosyphons. J. Heat Transf. 107, 826–832.

Creveling, H.F., De Paz, J.F., Baladi, J.Y., Schoenhals, R.J., 1975. Stability characteristics of a single-phase free convection loop. J. Fluid Mech. 67, 65–84.

De Nevers, N., 1970. Fluid mechanics. Addison-Wesley Series in Chemical Engineering, Addison-Wesley Pub. Co.

Di Marcello, V., Cammi, A., Luzzi, L., 2010. A generalized approach to heat transfer in pipe flow with internal heat generation. Chem. Eng. Sci. 65, 1301–1310.

Fiorina, C., Cammi, A., Luzzi, L., Mikityuk, K., Ninokata, H., Ricotti, M., 2014. Thermal-hydraulics of internally heated molten salts and application to the Molten Salt Fast Reactor. J. Phys.: Conf. Ser. 501, 1–10.

GIF, 2013. Generation IV International Forum Annual Report. URL: ⟨https://www.gen-4.org/gif/jcms/c_60764/gif-2013-annual-report⟩.

Gorman, M., Widmann, P., Robbins, K., 1986. Nonlinear dynamics of a convection loop: a quantitative comparison of experiment with theory. Physica D: Nonlinear Phenom. 19, 255–267.

Hallinan, K., Viskanta, R., 1986. Heat Transfer from a Rod Bundle Under Natural Circulation Conditions. Division of Accident Evaluation, Office of Nuclear Regulatory Research, U.S. Nuclear Regulatory Commission.

IAEA, 2005. Natural Circulation in Water Cooled Nuclear Power Plants Phenomena, Models and Methodology for System Reliability Assessments, IAEA-TECDOC-1474. Vienna, Austria.

Keller, J.B., 1966. Periodic oscillations in a model of thermal convection. J. Fluid Mech. 26, 599–606.

Luzzi, L., Aufiero, M., Cammi, A., Fiorina, C., 2012. Thermo-Hydrodynamics of Internally Heated Molten Salts for Innovative Nuclear Reactors. Hydrodynamics – Theory and Model, InTech, Rijeka, Croatia.

Luzzi, L., Cammi, A., Di Marcello, V., Fiorina, C., 2010. An approach for the modelling and the analysis of the MSR thermo-hydrodynamic behaviour. Chem. Eng. Sci. 65, 4873–4883.

MacCormack, R., 1969. The effect of viscosity in hypervelocity impact cratering. In: AIAA Hypervelocity Impact Conference, pp. 69–354.

MATLAB, 2013. The MathWorks, Inc., Natick, Massachussetts, United States. Misale, M., Ruffino, P., Frogheri, M., 2000. The influence of the wall thermal capacity and axial conduction over a single-phase natural circulation loop: 2-D numer-ical study. Heat Mass Transf. 36, 533–5396.

Perry, R., Green, D., 2008. Perry's Chemical Engineers' Handbook, eighth ed. McGraw-Hill, New York.

Pini, A., Cammi, A., Luzzi, L., Ruiz, D.E., 2014. Linear and nonlinear analysis of the dynamic behaviour of natural circulation with internally heated fluids. In: Proceedings of the 10th International Topical Meeting on Nuclear Thermal-Hydraulics, Okinawa, Japan, December 14–18, Paper NUTHOS10-1074, pp. 1–13.

Serp, J., Allibert, M., Beneš, O., Delpech, S., Feynberg, O., Ghetta, V., Heuer, D., Holcomb, D., Ignatiev, V., Kloosterman, J.L., Luzzi, L., Merle-Lucotte, E., Uhlíř, J., Yoshioka, R., Zhimin, D., 2014. The Molten Salt Reactor (MSR) in generation IV: overview and perspectives. Prog. Nucl. Energy 77, 308–319 URL: ⟨http://www.sciencedirect. com/science/article/pii/S0149197014000456⟩, doi: http://dx.doi.org/10.1016/j.pnucene.2014.02.014.

Swapnalee, B., Vijayan, P., 2011. A generalized flow equation for single phase natural circulation loops obeying multiple friction laws. Int. J. Heat Mass Transf. 54, 2618–2629.

Vijayan, P., 2002. Experimental observations on the general trends of the steady state and stability behaviour of single-phase natural circulation loops. Nucl. Eng. Des. 215, 139–152.

Vijayan, P., Austregesilo, H., Teschendorff, V., 1995. Simulation of the unstable oscillatory behavior of single-phase natural circulation with repetitive flow reversals in a rectangular loop using the computer code athlet. Nucl. Eng. Des. 155, 623–641.

Vijayan, P., Sharma, M., Saha, D., 2007. Steady state and stability characteristics of single-phase natural circulation in a rectangular loop with different heater and cooler orientations. Exp. Therm. Fluid Sci. 31, 925–945.

Vijayan, P.K., Nayak, A.K., Saha, D., Gartia, M.R., 2008. Effect of loop diameter on the steady state and stability behaviour of single-phase and two-phase natural circulation loops. Sci. Technol. Nucl. Install, http://dx.doi.org/10.1155/2008/ 672704.

Welander, P., 1967. On the oscillatory instability of a differentially heated fluid loop. J. Fluid Mech. 29, 17–30.

Wu, Q., Sienicki, J.J., 2003. Stability analysis on single-phase natural circulation in Argonne lead loop facility. Nucl. Eng. Des. 224, 23–32.